Activation of quartz flotation by Cu²⁺, Ni²⁺ in the sodium ethylxanthogenate (EX) system

Yang Liu [1], Xiong Tong [1,2], Rui-Qi Xie [1,2], Xian Xie [1,2], Qiang Song [1], Pei-Qiang Fan [1]

[1] Faculty of Land Resource Engineering, Kunming University of Science and Technology, Kunming 650093, Yunnan, China

[2] State Key Laboratory of Complex Nonferrous Metal Resources Clean Utilization, Kunming University of Science and Technology, Kunming 650093, Yunnan, China

Corresponding author: kgxiongtong@163.com e-mail (Xiong Tong)

Abstract: During the flotation of metal sulfide minerals, due to the interference of unavoidable ions, the quartz also partially floats in some cases. The studies on the mechanism of quartz being activated and floating up are still insufficient. In this study, the influence of the Cu^{2+} and Ni^{2+} unavoidable ions on the floatation of quartz was studied by micro-flotation experiments, adsorption detection, zeta potential measurement, solution composition calculation, infrared spectroscopy (FT-IR) and X-ray photoelectron spectroscopy (XPS) analyses, and atomic force microscopy (AFM) observation. This provides a theoretical reference for further understanding the mechanism of sodium ethylxanthogenate and quartz surface, as well as the development of a new quartz depressant. The results of flotation showed that after activation by Cu^{2+} (1×10^{-4} mol/dm³) and Ni^{2+} (5×10^{-5} mol/dm³), the quartz was captured by sodium ethylxanthogenate (EX: 1.4×10^{-4} mol/dm³) under alkaline conditions (pH=10), while the best recoveries were obtained as 80% and 43%, respectively. The results of adsorption and zeta potential measurements showed that the precipitation rate of Cu^{2+} was greater than that of Ni^{2+} under alkaline conditions. Additionally, both Cu^{2+} and Ni^{2+} electrostatically adsorbed on the quartz surface and changed the zeta potential of quartz. The solution composition calculation further showed that $Cu(OH)^+$, $Cu(OH)_{2(s)}$, and $Ni(OH)^+$, $Ni(OH)_{2(s)}$ were the main components in the solution under alkaline conditions. The FT-IR and XPS analyses and AFM observations demonstrated that Cu and Ni species adsorbed on O atoms on the quartz surface, providing active sites for EX adsorption, and EX combines with Cu and Ni species on the quartz surface to generate -O-Cu-EX and -O-Ni-EX complexes. Finally, the quartz floated up due to the formation of hydrophobic products and firm adsorption.

Keywords: quartz, flotation, ions activation, sodium ethylxanthogenate (EX), adsorption mechanism

1. Introduction

Nickel is an important strategic metal, and it is mainly used in the production of non-ferrous alloys in the aerospace industry (Guo et al., 2011). This product is crucial for industrial and military manufacturing. Nickel sulfide ore is the main nickel-containing resource, accounting for approximately 91% of the total nickel reserves (Watling, 2008). Copper is also an indispensable and important non-ferrous metal for modern industry, and has great strategic value. Copper resources with great utilization value exist in nature in the form of copper sulfide or copper oxide (Liu et al., 2019). When copper and nickel co-exist, they often exist in the form of sulfide ore and contain many rare elements such as copper, nickel, and cobalt, that have important mining value (Cameron et al., 2009).

In flotation of various sulfide ores such as galena, sphalerite, copper-nickel sulfide, and pyrite, quartz is often considered a gangue mineral (Liu et al., 2013; Zhao et al., 2020; Mweene et al., 2021; Nowosiel et al., 2022). Moreover, quartz is naturally hydrophilic and it has a large surface electronegativity above pH ~ 2, 5 (Liu et al., 2022). Therefore, it cannot float only by anionic collectors in the entire pH range. Many studies have shown that quartz can be activated by metal ions (Zn^{2+}, Pb^{2+}, Cu^{2+}, Fe^{3+}, Al^{3+}, Mg^{2+}, Ca^{2+}) and then floated by adding anionic collectors (He et al., 2022; Wang et al., 2022; Zhang et al., 2022;

Wang et al., 2022). Due to the slight dissolution of metal ions in metal sulfides or oxides, quartz is activated by unavoidable ions. It then floats up with anionic collectors, which results in its appearance in concentrates (Fornasiero and Ralston, 2009).

To better separate quartz from other minerals and prevent it from being accidentally activated, many studies were recently conducted on the depression of quartz (Yang and Wang. 2019; Liu et al., 2019; Zhao et al., 2022). The studies on the dispersion and depression mechanism of sodium silicate on quartz show that sodium silicate forms $SiO(OH)_3^-$ and $Si(OH)_4$ adsorption layers on the quartz surface, preventing the contact of Ca^{2+}, Mg^{2+}, and collectors with quartz (Hao et al., 2021). The citric acid depressant will greatly reduce the floatability of quartz. It can desorb Ca^{2+} adsorbed on the quartz surface and prevent the subsequent adsorption of sodium oleate (Wang et al., 2019). In the sodium oleate system, sodium alginate will form calcium alginate-calcium oleate complexes with Ca^{2+}. In addition, sodium alginate will desorb the pre-adsorbed sodium oleate from the mineral surface, and reduce the hydrophobicity of the mineral surface (Wang et al., 2021).

Although many of these studies have reported the positive effect of metal ions on the adsorption of anionic surfactants to quartz surfaces, the flotation performance of xanthate surfactants in metal ions and quartz systems has been rarely explored. In this study, the activation mechanism of Cu^{2+} and Ni^{2+} on quartz flotation under alkaline conditions was analyzed. Moreover, the influence of EX on the quartz flotation under certain Cu^{2+} and Ni^{2+} concentrations and a certain pH range was characterized by micro-flotation experiments. In addition, through zeta potential measurement, FT-IR and X-ray photoelectron spectroscopy (XPS) analyses, and atomic force microscopy (AFM) observation, the interaction sites and reaction products of agents and metal ions with mineral surfaces were revealed. Based on this study, the reasons why quartz may float during the flotation of metal sulfide ores were explained. This study provides novel ideas for the research and development of new quartz depressants.

2.   Materials and methods

2.1. Materials

Quartz ore from Laos was hand-selected to remove impurities, crushed, and then ground with a porcelain ball mill. After sieving, a 38-74 µm particle size sample was obtained as a pure mineral for testing, and the purity of the quartz was greater than 99% (Zhou et al., 2022). The collectors used in the experiment were sodium ethylxanthogenate purchased from Tianjin Kermel Chemical Reagents Company in China, the frother was isobutyl methyl carbinol (MIBC), the pH regulators were HCl and NaOH, and the activators were $CuCl_2 \cdot 2H_2O$ and $NiCl_2 \cdot 6H_2O$, all purchased from Aladdin Chemical in China. The agents were all analytically pure, and deionized water was used for flotation.

2.2. Methods

2.2.1. Pure mineral flotation experiments

Quartz flotation experiments were performed in the XFGCII-35 laboratory flotation machine at room temperature (25°C). The impeller speed was 1500 r/min, and 2 g of test ore samples were weighed each time and added to a 40 cm³ flotation cell. 38 cm³ of deionized (DI) water was also added (Cao et al., 2022). HCl or NaOH pH regulators were used to mix for 2 min. $CuCl_2$ or $NiCl_2$ was then used and stirring is performed for 3 min. Collector sodium ethylxanthogenate was added for 3 min, and finally, frother was added and stirring was performed for 2 min (Zhang et al., 2022).

2.2.2. Adsorption detection

2 g of pure quartz minerals and 38 cm³ of DI water were added to a 40 cm³ flotation machine. The pH of the pulp was then adjusted with HCl or NaOH solution, metal ions were added, and stirring was performed for 2 min. The pulp was centrifuged with the TG-21WC, and the supernatant was taken to detect the metal ion concentration with an atomic absorption spectrophotometer. The strength of the mineral surface to adsorb metal ions is characterized by the adsorption precipitation rate (ρ_{AP}), which is defined as Eq. (1):

$$\rho_{AP} = \frac{(c_0 - c)}{c_0} \cdot 100\% \tag{1}$$

where c_0 is the initial concentration of metal ions and c is the concentration of metal ions in the filtrate. The larger the ρ_{AP} value, the more metal ions adsorb on the mineral surface (Guan et al., 2022).
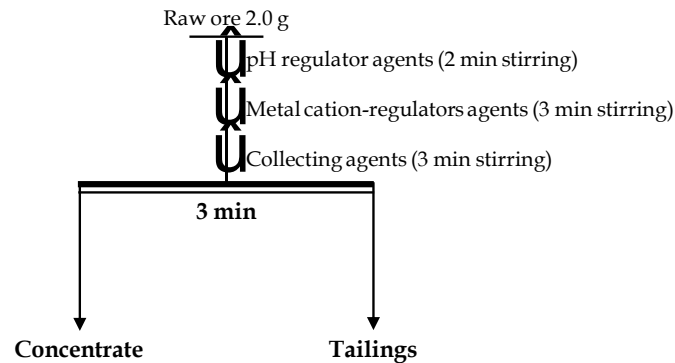

Fig. 1. Flowchart of the quartz flotation experiments

2.2.3. Zeta potential measurements

The pure quartz mineral was taken, and ground to a particle size of less than 2 μm. 40 mg was weighed each time and placed in a beaker. 40 cm³ pulp with potassium chloride was prepared, and the pH value was adjusted with HCl or NaOH. Flotation reagents were added in sequence according to the flotation conditions. After stirring on a magnetic stirrer for 6 min, the above sample was added to the sample cell, and measured by a Brookhaven ZetaPlus Analyzer. The measurement was repeated three times for each sample, and the average value was considered as the test result (Wang et al., 2021; Dong et al., 2022).

2.2.4. Solution composition calculation

The Visual MINTEQ 3.1 chemical equilibrium software was used to calculate the dominant components of Cu^{2+} and Ni^{2+} solutions at corresponding concentrations, and the Origin 2019 software was used to draw the curve.

2.2.5. FT-IR spectrum measurements

2 g of pure quartz mineral with a particle size of less than 2 μm was weighed. The pH was adjusted to 10. Then, Cu^{2+} (1×10^{-4} mol/dm³) or Ni^{2+} (5×10^{-5} mol/dm³) and sodium ethylxanthogenate with a concentration of 1.4×10^{-4} mol/dm³ were added. Full stirring was applied and the solution was let to settle for 5 min. Afterwards, a plastic tip dropper was used to suck out the supernatant. Full washing was performed with deionized water. After waiting for the quartz to naturally dry, a Nicolet FTIR-670 Fourier transform infrared spectrometer was used, and an infrared spectrum test was conducted using the potassium bromide tablet method (Xie et al., 2021).

2.2.6. XPS analysis

The XPS test was performed using a PHI5000 Versaprobe-II X-ray photoelectron spectrometer. 1 g of quartz was first weighed into a beaker. The pH was then adjusted to 10 with NaOH. A certain concentration of flotation agents was added in sequence according to the flotation conditions, and stirring was performed using a magnetic stirrer for 6 min. Filtering followed by washing was then applied for the minerals with deionized water, and finally, the XPS test was performed after vacuum drying at 40°C for 10 h. The XPS test conditions are monochromatic AlKα ray light source, C 1s calibration value of 284.8 eV, and Avantage was used for spectral peak analysis and spectral peak fitting (Lv et al., 2021).

2.2.7. AFM observation

The pure quartz slices were ground and polished, ultrasonically cleaned for 5 min in 30 KHz, and then the samples were dried and placed in a beaker. The preparation and pH of the flotation solution were

similar to the optimal conditions for the flotation experiment. After the pure quartz slices were reacted with the solution for 20 min, they were dried in a low temperature (40℃) vacuum oven for 12 h. Finally, the AFM image of quartz and Fig. of cross-section height with a scanning range of 5 μm × 5 μm were obtained by SPA-400 atomic force microscope (Xie et al., 2021).

3.   Results and discussion

3.1. Pure mineral flotation experiments

The influence of the pH value on the floatability of quartz under different concentrations of Cu^{2+} and Ni^{2+}, for a concentration of sodium ethylxanthogenate of $1.4×10^{-4}$ mol/dm³ and dosage of isobutyl methyl carbinol (MIBC) of 15 mg/dm³, was first observed. The results are shown in Fig. 2. When there is no Cu^{2+} and Ni^{2+} in the pulp, the recovery rate of quartz is lower than 4%. The surface of unactivated quartz is completely hydrophilic, and the entrainment of bubbles causes the floating of quartz.

The recovery rate of quartz under the same pH condition shows that when the Cu^{2+} concentration ($1×10^{-4}$ mol/dm³) is close to the sodium ethylxanthogenate concentration, the recovery rate of quartz is the highest (almost 80%), as shown in Fig. 2(a). When the concentration of Cu^{2+} increased to $5×10^{-4}$ mol/dm³, the adsorption of Cu^{2+} on the quartz surface reached saturation, and the recovery rate slightly decreased when it was alkaline. When the concentration of Cu^{2+} is low ($5×10^{-5}$ mol/dm³), the adsorption of Cu^{2+} on the quartz surface is not saturated, and the activation effect is not clear. In addition, in the whole pH range, for different concentrations of Cu^{2+} in the solution, the recovery of quartz first increases with the increase of the pH value, reaches the maximum value around pH = 10, and then shows a downward trend. That is, under the conditions of suitable Cu^{2+} concentration and alkaline pH value, Cu^{2+} has a great activation effect on quartz.
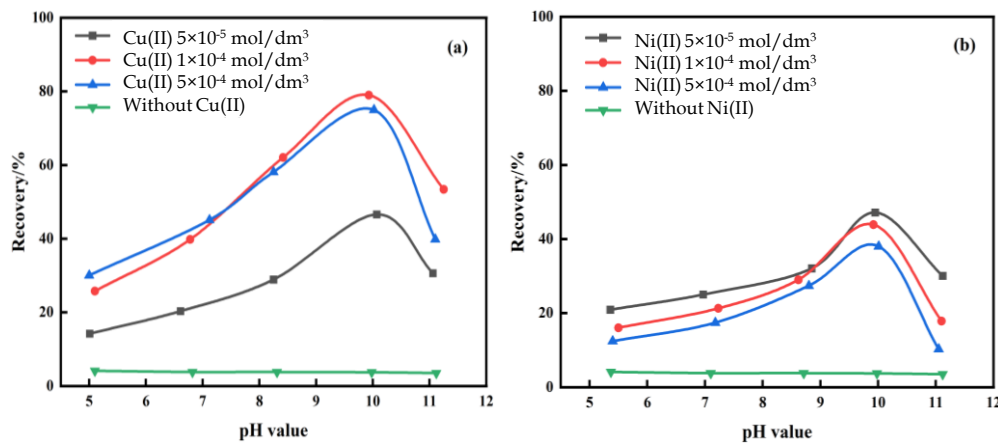

Fig. 2. Influence of the pH value and metal ion concentration on the recovery rate of quartz: (a) Cu^{2+}; (b) Ni^{2+} (EX $1.4×10^{-4}$ mol/dm³)

Compared with the activation effect of Cu^{2+}, the activation effect of Ni^{2+} is much weaker. When the Ni^{2+} concentration is low ($5×10^{-5}$ mol/dm³), the Ni^{2+} adsorbed on the quartz surface reaches saturation, and at the optimum pH (pH=10), the highest recovery rate of quartz is almost 43%, as shown in Fig. 2(b). On the other hand, at other higher Ni^{2+} concentrations, the recovery of quartz is slightly lower at the same pH, due to the consumption of sodium ethylxanthogenate by excess of Ni^{2+}. Similarly, in the whole pH range, for different concentrations of Ni^{2+} in the solution, the recovery of quartz first increases with the increase of the pH value, reaches a maximum value around pH = 10, and then shows a downward trend. The results show that under the conditions of suitable Ni^{2+} concentration and alkaline pH value, Ni^{2+} has a certain activation effect on quartz.

3.2. Adsorption detection

The percentages of Cu^{2+} and Ni^{2+} adsorption and precipitation on the quartz surface under different pH conditions are shown in Fig. 3. In the experiments, the initial concentrations of Cu^{2+} and Ni^{2+} metal ions were $1×10^{-4}$ mol/dm³ and $5×10^{-5}$ mol/dm³, respectively.

It can be seen from Fig. 3 that in the pH range of 5-10, the adsorption of Cu^{2+} ions onto quartz increases with the increase of the pH value. When pH = 10, the adsorption of Cu^{2+} on the mineral surface reaches the highest value. In the pH range of 5-10, the adsorption of Ni^{2+} onto quartz gradually increases, and the adsorption reaches the highest value at around pH = 10. Too acidic or too basic pH conditions are not conducive to the adsorption of Cu^{2+} and Ni^{2+} on the quartz surface, and the adsorption law of Cu^{2+} and Ni^{2+} on the quartz surface is consistent with the phenomenon of quartz flotation
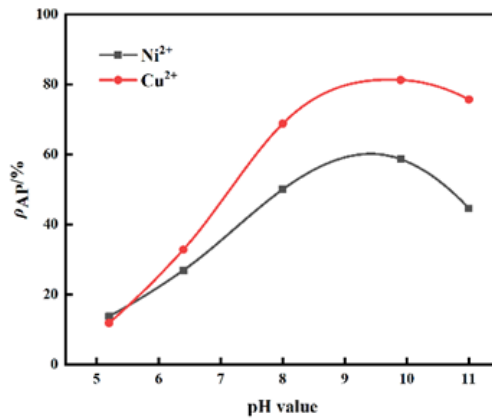

Fig. 3. Percentage of metal ions adsorbed and precipitated on the quartz surface under different pH conditions
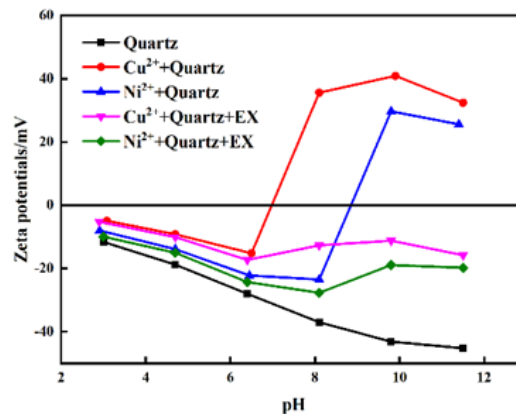
.

Fig. 4. Effects of the pH and Cu^{2+}, Ni^{2+} on the zeta potential of quartz

3.3. Zeta potential measurements

The impacts of a certain concentration of Cu^{2+} (1×10^{-4} mol/dm^3) and a certain concentration of Ni^{2+} (5×10^{-5} mol/dm^3) on the zeta potential of quartz were studied. The obtained results are shown in Fig. 4. The zeta potential of quartz is negative and decreases with the increase of the pH value. After adding Cu^{2+} and Ni^{2+}, the electrostatic adsorption leads to the increase of the zeta potential of the quartz surface. After adding sodium ethylxanthogenate, the quartz surface generates corresponding copper (II) xanthate and nickel (II) xanthate, which also reduces the zeta potential. When the pH of the pulp is low, the adsorption amount of Cu^{2+} and Ni^{2+} on the quartz surface is small, and the increase of zeta potential is not clear. When pH = 10, the hydroxide precipitates or hydroxyl complexes of Cu^{2+} and Ni^{2+} can be adsorbed on the mineral surface, which increases the zeta potential of the quartz surface. This phenomenon proves that the electrostatic adsorption of Cu^{2+} and Ni^{2+} leads to the change of the zeta potential of the quartz surface.

3.4. Analysis of the solution composition calculation

The predominant components in the calculated solution, for a concentration of Cu^{2+} of 1×10^{-4} mol/dm^3, are shown in Fig. 5(a). When the pH of the solution is less than 6.3, the main component in the solution

is Cu^{2+}, and the pH value range of quartz with good floatability corresponds to the distribution of Cu hydroxide precipitation or hydroxyl complex species. The pure mineral flotation and zeta potential tests show that when the pH of the solution is less than 6.3, Cu^{2+} cannot be fully adsorbed on the quartz surface, and the activation effect is poor. When the pH of the solution is almost 10, the dominant components in the solution are $Cu(OH)_{2(s)}$ and $Cu(OH)^+$, and the copper species attaches to the quartz surface and reacts with sodium ethylxanthogenate to activate the quartz flotation (Liu et al., 2016).
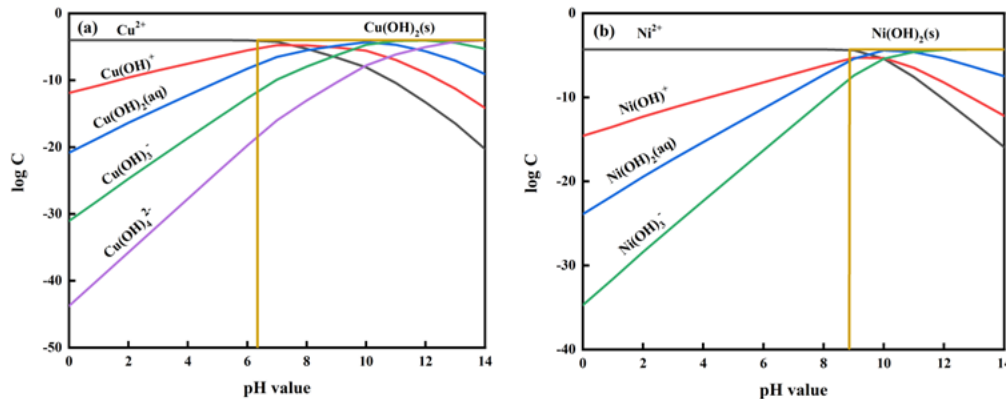

Fig. 5. Species distribution diagram of Cu^{2+} and Ni^{2+} in the solution function of the pH: (a) Cu^{2+}; (b) Ni^{2+}

The dominant components in the calculated solution, for Ni^{2+} concentration of 5×10^{-5} mol/dm³, are shown in Fig. 5(b). It can be seen that when the pH of the solution is less than 8.4, the main component is Ni^{2+}, and the pH range of quartz with good floatability corresponds to the distribution of Ni hydroxide precipitation or complex species. The pure mineral flotation and zeta potential tests show that when the pH of the solution is less than 8.4, Ni^{2+} cannot be fully adsorbed on the quartz surface, and the activation effect is not clear. When the pH of the solution is almost 10, the dominant components are $Ni(OH)_{2(s)}$ and $Ni(OH)^+$, and the nickel species attach to the quartz surface and react with sodium ethylxanthogenate to activate the quartz flotation (Zhang et al., 2021).

3.5. FT-IR spectroscopic analysis

Infrared spectrum analysis was conducted to study the reaction of quartz with sodium ethylxanthogenate activated by Cu^{2+} and Ni^{2+}. The obtained results are shown in Figs. 6 and 7. The spectral line in Fig. 6(a) is the infrared spectrum of pure quartz, which is the Si-OH stretching vibration absorption peak at 3448 cm⁻¹. The broad and strong absorption peak at 1085 cm⁻¹ is the Si-O asymmetric stretching vibration absorption peak, and 779 cm⁻¹ is the absorption peak of Si-O symmetrical stretching vibration (Xie et al., 2021). Spectral line (b) is the infrared spectrum of quartz + sodium ethylxanthogenate. There is no characteristic peak of sodium ethylxanthogenate functional group and no shift of the characteristic peak of quartz, which indicates that sodium ethylxanthogenate has no adsorption effect on the quartz surface. Spectral line (c) is the infrared spectrum of sodium ethylxanthogenate, 1182 cm⁻¹ and 1106 cm⁻¹ are respectively the asymmetric stretching vibration peak and symmetric stretching vibration peak of the C-O-C bond, and 1065 cm⁻¹ is the C=S bond stretching vibration peak (Luo et al., 2022). Spectral line (d) is the infrared spectrum of the interaction between quartz and sodium ethylxanthogenate after Cu^{2+} activation, in which the C-O-C bond asymmetric stretching vibration peak and symmetric stretching vibration peak of sodium ethylxanthogenate moved to 1123 cm⁻¹ and 1083 cm⁻¹, and the C=S bond stretching vibration peak moved to 1076 cm⁻¹. The shift of characteristic peaks indicated that after activation by Cu^{2+}, sodium ethylxanthogenate produced hydrophobic copper (II) xanthate on the quartz surface, and the chemical adsorption was strong (Zhang et al., 2022).

The spectral lines (a), (b), and (c) in Fig. 7 are the infrared spectra of pure quartz, quartz + sodium ethylxanthogenate, and sodium ethylxanthogenate, respectively. Spectral line (d) is the infrared spectrum of the interaction between quartz and sodium ethylxanthogenate after Ni^{2+}activation. The C-O-C bond asymmetric stretching vibration peak and symmetric stretching vibration peak of sodium ethylxanthogenate moved to 1250 cm⁻¹ and 1163 cm⁻¹, and the C=S bond stretching vibration peak

moved to 1083 cm^{-1}. The shift of the characteristic peak indicates that after Ni^{2+}activation, nickel (II) xanthate acts on the surface of quartz by chemical adsorption, causing part of the quartz to float (Naklicki et al., 2002).
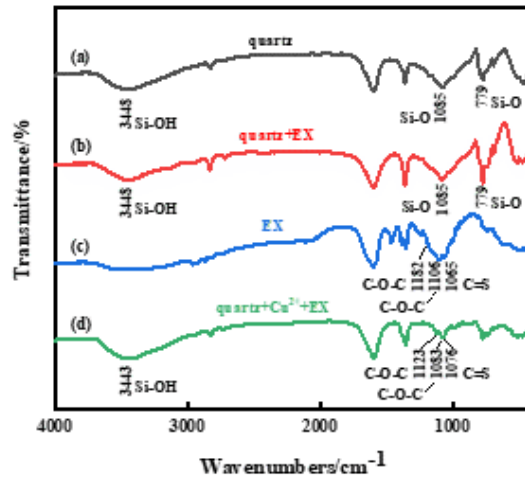
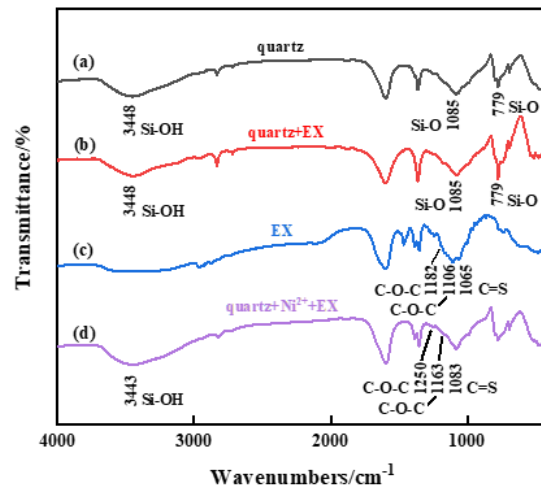Fig. 6. Infrared spectra of the interaction between quartz and sodium ethylxanthogenate activation by Cu^{2+}

Fig. 7. Infrared spectra of the interaction between quartz and sodium ethylxanthogenate activation by Ni^{2+}

3.6. XPS analysis

The XPS energy spectrum was used to analyze the action mode and adsorption structure of Cu^{2+}, Ni^{2+}, and sodium ethylxanthogenate on the quartz surface. The obtained results are shown in Table 1, and Fig. 8 (a), (b), (c), (d), and (e) show the XPS spectra of quartz, EX, quartz+EX, quartz+Cu^{2+}+EX, and quartz+Ni^{2+}+EX, respectively. The survey spectra of quartz are shown in curve (a) in Fig. 8, where Si(2p), O(1s), O KL1, and C(1s) appear, indicating that the quartz is a pure mineral. Curve (b) shows the survey spectra of EX, where S(2p), Na(1s), O(1s), and C(1s) appear. The XPS survey spectra after the action of quartz and EX is shown in curve (c), and no new peaks appear compared with the XPS survey spectra of quartz. In curves (d) and (e), the peaks of Cu(2p) and Ni(2p) respectively appear, and the peaks of S(2p) belonging to EX appear together, which proves that copper (II) xanthate and nickel (II) xanthate are adsorbed on the quartz surface.

As seen from Table 1, EX has a very low influence on the binding energy of the outer orbital electrons of quartz, and will not adsorb to quartz. After the quartz surface was treated with Cu^{2+} and Ni^{2+}, EX was added, the peaks of Cu (atomic concentration 3.54%) and Ni (atomic concentration 2.58%) appeared, and the S atomic concentrations were 1.43% and 1.25%, respectively. This indicates that Cu^{2+} and Ni^{2+} can be adsorbed on the quartz surface and provide active sites so that EX can be adsorbed on the quartz surface (Dong et al., 2022).
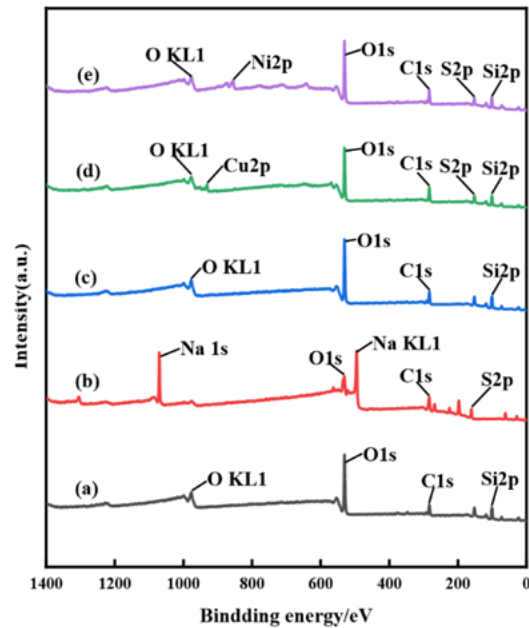
Fig. 8. XPS survey spectra of quartz with the treatment of agents (a): Quartz; (b): EX; (c): Quartz+EX;
(d): Quartz+Cu^{2+}+EX; (e): Quartz+Ni^{2+}+EX

Table 1. The atomic orbital binding energies and atomic contents of elements under the action of quartz and different agents

Sample	Binding energy (eV)						At (%)					
	O(1s)	C(1s)	Si(2p)	S(2p)	Cu(2p)	Ni(2p)	O(1s)	C(1s)	Si(2p)	S(2p)	Cu(2p)	Ni(2p)
Quartz	532.16	284.86	102.95	–	–	–	50.84	26.02	23.14	–	–	–
EX	532.96	285.47	–	162.37	–	–	27.12	39.75	–	9.79	–	–
Quartz+EX	532.14	284.84	102.89	–	–	–	49.86	27.27	22.87	–	–	–
Quartz+Cu^{2+}+EX	532.29	284.72	102.96	162.71	933.07	–	45.46	31.08	19.62	1.43	3.54	–
Quartz+Ni^{2+}+EX	532.17	284.87	103.02	162.58	–	853.61	46.16	30.17	18.85	1.25	–	2.58

In Fig. 9, the Si2p orbital and O1s orbital are subjected to peak fitting, and the Si2p high-resolution spectra of (a), (b), and (c) correspond to untreated quartz (Liu et al., 2022), Cu^{2+}+EX-treated quartz, and Ni^{2+}+EX treated quartz, respectively. The peaks of Si2p orbitals have no clear shift, which indicates that the agent does not interact with the Si atoms on the mineral surface (Han et al., 2022). The O1s orbital high-resolution spectra of (d), (e), and (f) correspond to untreated quartz, Cu^{2+}+EX-treated quartz, and Ni^{2+}+EX-treated quartz, respectively. After treatment with Cu^{2+}, the O1s orbital peak shifted, and the spectral peaks were fitted to yield C-O-C species (532.87 eV) belonging to EX, Si-O species (532.1 7eV), and Cu-O species (531.18 eV). After Ni^{2+} treatment, the O1s orbital peak shifted, and the spectral peaks were fitted to produce C-O-C species (533.59 eV) belonging to EX, Si-O species (532.27 eV), and Ni-O species (531.12 eV). This phenomenon proves that the Cu^{2+} and Ni^{2+} metal ions have chemical adsorption on the quartz surface, which results in the formation of hydrophobic copper (II) xanthate and nickel (II) xanthate, and the adsorption is stable (Wang et al., 2022).

The spectral peaks of the activated quartz C(1s) orbital, Cu(2p) orbital, and Ni(2p) orbital were fitted to analyze the reaction products and the mode of action, as shown in Fig. 10. The C1s high-resolution spectrum of the interaction between quartz and EX after activation by Cu^{2+} is shown in Fig. 10(a). After peak fitting, C-O-C species (286.41 eV) and C-C/C-H species (284.73 eV) belonging to EX appeared. Fig. 10(b) presents the C1s orbital high-resolution spectrum of the interaction between quartz and EX after activation by Ni^{2+}. After peak fitting, C-O-C species (286.21 eV) and C-C/C-H species (284.78 eV) belonging to EX appeared. This confirms the adsorption of EX on the activated quartz surface. Fig. 10(c)
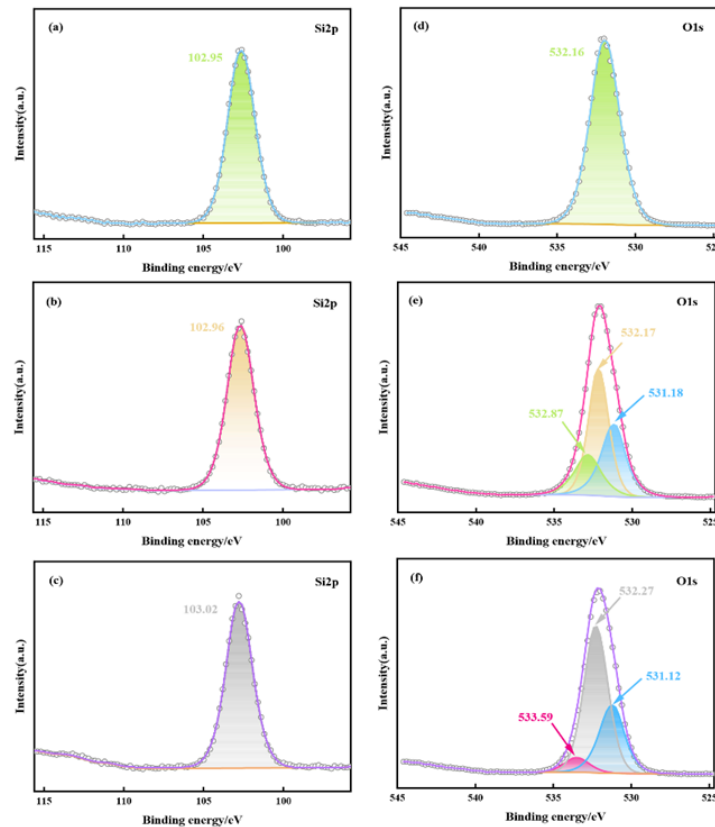
Fig. 9. Comparison between the Si(2p) and O(1s) XPS high-resolution spectra of quartz and EX reaction(a): Quartz
Si(2p); (b): Quartz+ Cu^{2+}+EX Si(2p); (c): Quartz+Ni^{2+}+EX Si(2p);
(d): Quartz O(1s); (e): Quartz+ Cu^{2+}+EX O(1s); (f): Quartz+Ni^{2+}+EX O(1s)

shows the spectral peak fitting of the Cu2p orbital of quartz after activation by Cu^{2+}. The bindingenergies of Cu2p$_{1/2}$ orbital and Cu2p$_{3/2}$ orbital are located at 952.63 eV and 932.87 eV, which belong to the Cu-S species adsorbed on the surface of quartz (Luo et al., 2022). The two peaks of Cu-O species are located at 955.36 eV and 935.55 eV (Zhao et al., 2022). Fig. 10(d) is the peak fitting of the Ni2p orbital of quartz after Ni^{2+} activation. It shows that the binding energies of the Ni2p$_{1/2}$ orbital and Ni2p$_{3/2}$ orbital are located at 869.78 eV and 852.12 eV, which belong to the Ni-S species adsorbed on the quartz surface. The two peaks of Ni-O species are located at 872.46 eV and 855.13 eV (Wang et al., 2021). This phenomenon shows that -O-Cu-S- bond and -O-Ni-S- bond structures are formed between the quartz surface and EX after activation by Cu^{2+} and Ni^{2+}, and the hydrophobic copper (II) xanthate and nickel (II) xanthate eventually lead to the floating of quartz.

3.7. AFM observation

The surface morphology of quartz interaction with Cu^{2+}, Ni^{2+}, and EX at pH = 10 was observed by AFM. The results are shown in Figs. 11 and 12. The untreated quartz surface is relatively flat, as shown in Figs. 11(a), (b), and (c). At a pH of 10, after Cu^{2+} treatment (Figs. 11(d), (e), and (f)), the quartz surface becomes rough and small plaques appear. It can be deduced from this solution composition analysis that the main component of these plaques is Cu(OH)$_{2(s)}$. After Cu^{2+} activation, EX was added. The AFM measurements are shown in Figs. 11(g), (h), and (i). At this time, the quartz surface was rougher, a large number of island-like plaques appeared, and the precipitates were more and larger, and they were formed by the adsorption of EX on the Cu species. The Cu species adsorbed on the quartz surface is the active site for EX adsorption, the surface product -Cu-EX is hydrophobic and causes a large amount of quartz to float up.

The untreated quartz surface is relatively flat, as shown in Figs. 11(a), (b), and (c). At a pH of 10, after Ni^{2+} treatment (Figs. 12(a), (b), and (c)), the quartz surface becomes rough and small plaques appear. It can be deduced from this solution composition analysis that the main component of these plaques was

$Ni(OH)_{2(s)}$. After the Ni^{2+} activation treatment, EX was added. The AFM measurements are shown in Figs. 12(d), (e), and (f). At this time, the quartz surface became rough, and several peaks appeared, but the number of the precipitates was small, which was formed by the adsorption of EX on a small part of Ni species. In addition, the adsorption amount of -Ni-EX is small, causing part of the quartz to float.
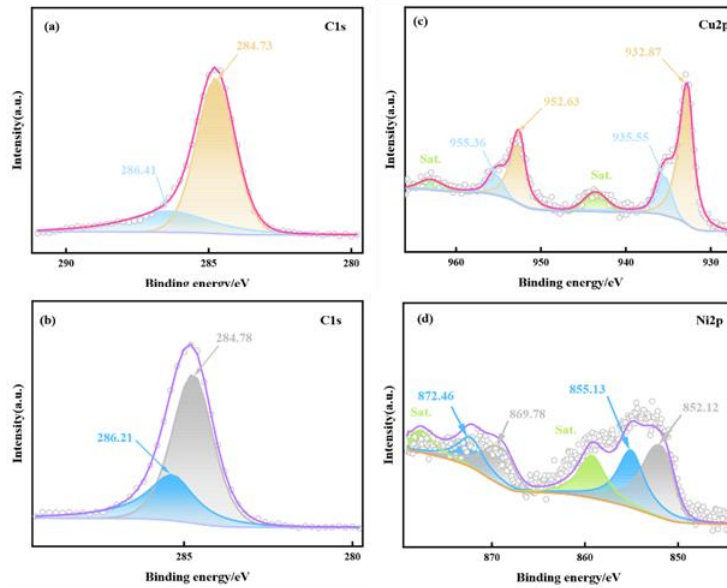

Fig. 10. Comparison between the XPS high-resolution spectra of the C(1s) orbital, Cu(2p) orbital, and Ni(2p) orbital of quartz after activation (a): Quartz+Cu^{2+}+EX C(1s); (b): Quartz+Ni^{2+}+EX C(1s); (c): Quartz+ Cu^{2+}+EX Cu(2p); (d) Quartz+ Ni^{2+}+EX Ni(2p)
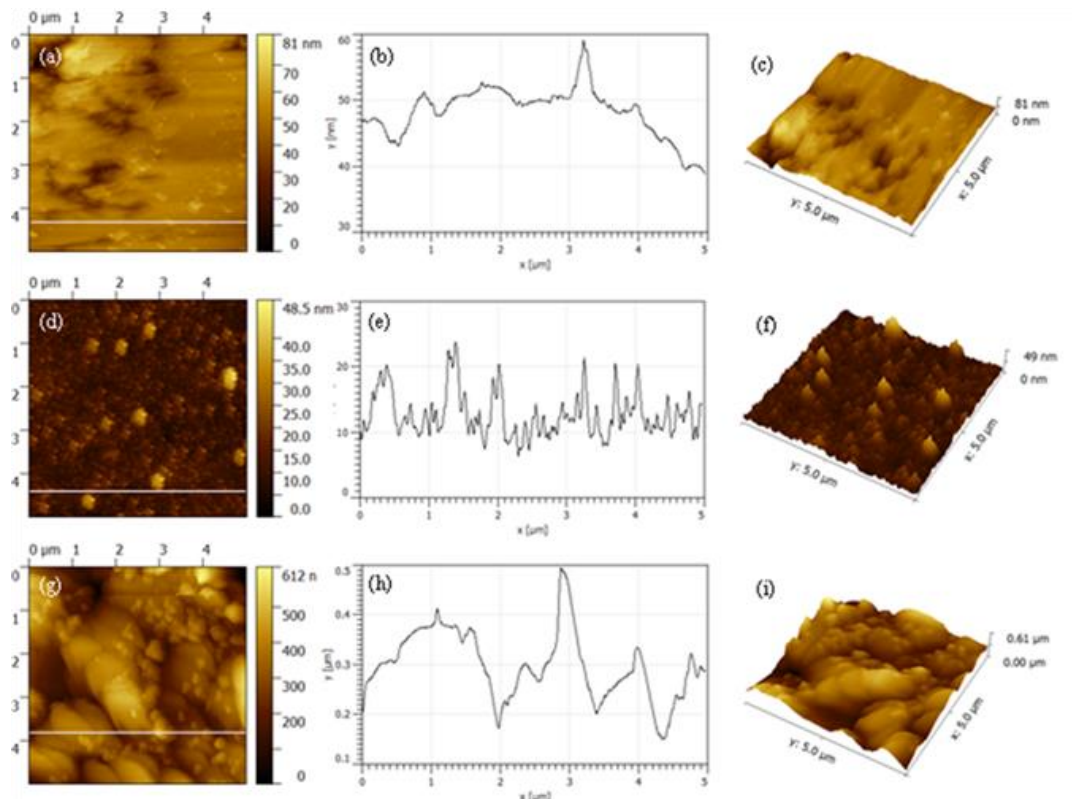

Fig. 11. Topographic height images of quartz surface: (a) 2D image of untreated quartz; (b) cross-section height of untreated quartz; (c) 3D image of untreated quartz; (d) quartz treated with Cu^{2+} 2D image; (e) cross-section height of Cu^{2+}-treated quartz; (f) 3D image of Cu^{2+}-treated quartz; (g) 2D image of Cu^{2+}+EX-treated quartz; (h) cross-section height of Cu^{2+}+EX-treated quartz; (i) 3D image of Cu^{2+}+EX-processed quartz
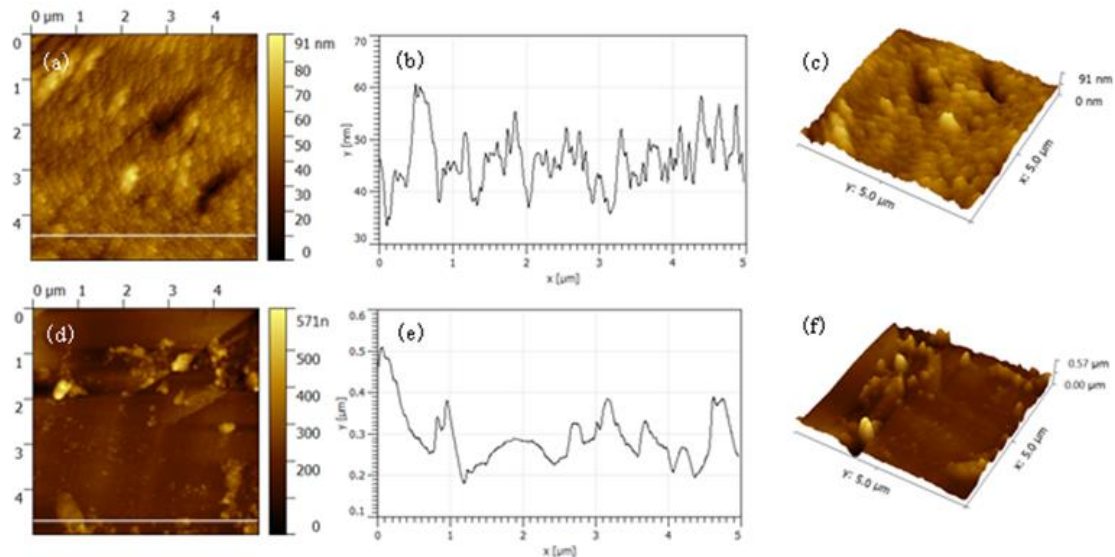
Fig. 12. Topographic height images of quartz surface: 3D image of untreated quartz; (a) quartz treated with Ni^{2+} 2D image; (b) cross-section height of Ni^{2+}-treated quartz; (c) 3D image of Ni^{2+}-treated quartz; (d) 2D image of Ni^{2+}+EX-treated quartz; (e) cross-section height of Ni^{2+}+EX-treated quartz; (f) 3D image of Ni^{2+}+EX-processed quartz

It can be deduced from the above observations that the surface roughness of the untreated quartz was increased after Cu^{2+} and Ni^{2+} activation. The surface roughness continued to increase after the EX addition in the presence of the ions. However, by comparing the activation effects of Cu^{2+} and Ni^{2+}, it was deduced that the quartz surface can adsorb more -Cu-EX after activation by Cu^{2+}. The number of -Cu-EX peaks is much more than that of -Ni-EX peaks, which confirms that the adsorption amount of EX on the quartz surface after Cu^{2+} activation is much larger than that after Ni^{2+} activation. This is consistent with the flotation experiment and the adsorption amount measurement results.
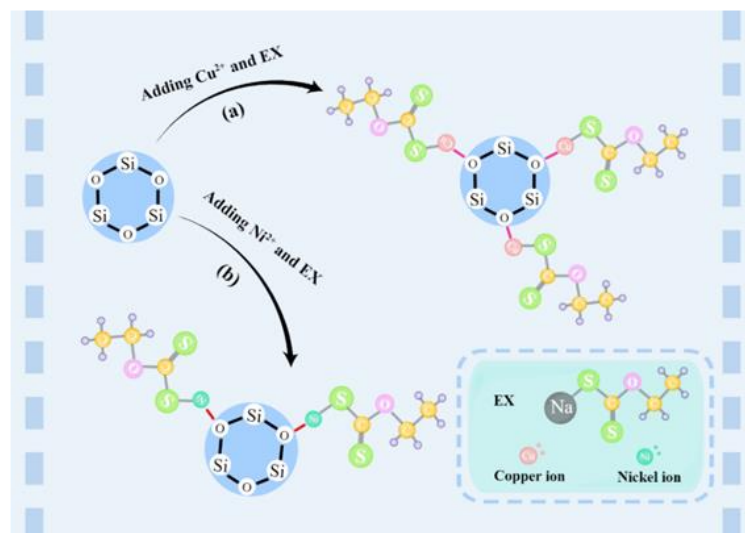

Fig. 13. Adsorption model of quartz surface: (a) Cu^{2+}+EX; (b)Ni^{2+}+EX

Based on the theoretical analysis, an adsorption model (Fig. 13) was developed to study the influence of EX on the floating of quartz after activation by Cu^{2+} and Ni^{2+}. It can be deduced that when there are Cu^{2+} and Ni^{2+} in the pulp and the pH of the pulp is 10, Cu(OH)$_{2(s)}$ and Ni(OH)$_{2(s)}$, respectively, generate electrostatic adsorption on the quartz surface, changing the zeta potential of the quartz. Subsequently, the S atoms in the EX molecules generate stable chemisorption with -O-Cu and -O-Ni species on the quartz surface to form hydrophobic stable complexes on it. Finally, the hydrophobic -CuEX and -NiEX species act on the quartz surface in a chemisorption manner and cause the quartz to float. The

adsorption measurements and AFM observations proved that the number of -CuEX species was greater than that of -NiEX species, and this phenomenon also corresponds to the flotation recovery. It can be deduced from all the phenomena that the promotion effect of Cu^{2+} on the adsorption of EX on quartz is much stronger than that of Ni^{2+}.

4. Conclusions

This study explores the impacts of Cu^{2+} and Ni^{2+} on the quartz surface properties and floatation. The microflotation recovery rate proves that sodium ethylxanthogenate floats the quartz after activation by Cu^{2+} and Ni^{2+} in the alkaline region. The recovery rates of quartz are respectively 80% and 43%, and the activation effect of Cu^{2+} is stronger than that of Ni^{2+}. The species distribution diagram of Cu^{2+} and Ni^{2+} indicates that $Cu(OH)^+$, $Cu(OH)_{2(s)}$, and $Ni(OH)^+$, $Ni(OH)_{2(s)}$ are the main components adsorbed on the quartz surface in the flotation pulp. They act as the active site for the reaction of the quartz surface with EX. The zeta potential and adsorption measurements showed that the Cu and Ni species acted on the quartz surface by electrostatic adsorption, and the adsorption of Cu^{2+} was greater than that of Ni^{2+}. The FT-IR test and XPS analysis demonstrated that the quartz surface was adsorbed with Cu and Ni species through O atoms. In addition, the Cu and Ni species adsorbed on the quartz surface chemisorbed with the S atoms of sodium ethylxanthogenate, which resulted in hydrophobic -CuEX and -NiEX species. Finally, the island-like precipitation patches and distribution of -CuEX and -NiEX species were observed on the quartz surface by AFM, which confirmed the different impacts of Cu^{2+} and Ni^{2+} on quartz floating. This theoretical study, aims at controlling the influence of unavoidable ions concentration and pulp pH in industrial production, to avoid creating good floating conditions for quartz. The mechanism of unavoidable ions activation of quartz was also studied, in order to provide a theoretical reference for the research and development of a new quartz depressant.

References

CAMERON, R.A., LASTRA, R., MORTAZAVI, S., BEDARD, P.L., MORIN, L., GOULD, W.D., KENNEDYA, K.J., 2009. *Bioleaching of a low-grade ultramafic nickel sulphide ore in stirred-tank reactors at eleVated pH*, Hydrometallurgy. 97, 213-220.

CAO, S.H., YIN, W.Z., YANG, B., ZHU, Z.L., SUN, H.R., SHENG, Q.Y., CHEN, K.Q., 2022. *Insights into the influence of temperature on the adsorption behavior of sodium oleate and its response to flotation of quartz*. Int. J. Min, Sci. Techno. 32, 399-409.

DONG, J.S., LIU, Q.J., SUBHONQULOV, S.H., SHENG, J., GAO, Y.L., LIU, M.L., 2022. *Research on the flotation of sphalerite and germanium-bearing sphalerite activated by copper ion and its mechanism difference*. Miner. Eng. 186. 107756.

DONG, J.S., LIU, Q.J., YU, L., SUBHONQULOV, S.H., 2022. *Activation mechanism of copper ion in arsenopyrite flotation in high pH value*. Miner. Eng. 179, 107465.

FORNASIERO, D., RALSTON, J., 2005. *Cu (II) and Ni (II) activation in the flotation of quartz, lizardite and chlorite*. Int. J. Miner. Process. 76, 75-81.

HAN, W.J., ZHU, Y.M., GE ,W.C., LIU, J., LI, Y.J., 2022. *Curdlan as a new depressant of hematite for quartz-hematite reVerse flotation separation*. Miner. Eng. 185, 107708.

GUAN, X.D., LI, P., LIU, W.K., CHANG, Q.Q., HAN, Y.W., ZHANG, J.K., ZHANG, H.L., LI, Q., ZHEN, S.L., 2022. *Adsorption mechanism of yttrium ions onto ion-adsorption type rare earths ore*. Sep. Purif. Technol. 299, 121641.

GUO, X.Y., SHI, W.T., LI, D., TIAN, Q.H., 2011. *Leaching behavior of metals from limonitic laterite ore by high pressure acid leaching*. T. Nonferr. Metal. Soc. 21, 191-195.

HAO, H.Q., CAO, Y.J., LI, L.X., FAN, G.X., LIU, J.T., 2021. *Dispersion and depression mechanism of sodium silicate on quartz: Combined molecular dynamics simulations and density functional theory calculations*. Appl. Surf. Sci. 537, 147926.

HE, J.F., CHEN, H., ZHANG, M.M., CHEN, L.H., YAO, Q.Y., DAI, Y.P., ZHU, L.T., LIU, C.G., 2022. *Combined inhibitors of Fe^{3+}, Cu^{2+} or Al^{3+} and sodium silicate on the flotation of fluorite and quartz*. Colloid. Surface. A. 643, 128702.

LEROY, P., MAINEULT, A., LI, S., VINOGRADOV, J., 2022. *The zeta potential of quartz. Surface complexation modelling to elucidate high salinity measurements*. Colloid. Surface. A. 650, 129507.

LIU, J., WEN, S.M., WU, D.D., BAI, S.J., LIU, D., 2013. *Determination of the concentrations of calcium and magnesium released from fluid inclusions of sphalerite and quartz*. Miner. Eng. 45, 41-43.

LIU, B., WANG, X.M., DU, H., LIU, J., ZHENG, S.L., ZHANG, Y., MILLER, J.D., 2016. *The surface features of lead activation in amyl xanthate flotation of quartz*. Int. J. Miner. Process. 151, 33-39.

LIU, J., LIU, G.Y., HUANG, Y.G., ZHANG, Z.Y., 2019. *Tetrazinan-thione collectors for copper oxide mineral: Synthesis and flotation mechanism*. Appl. Surf. Sci. 491, 624-632.

LIU, C., ZHU, G.L., SONG, S.X., LI, H.Q., 2019. *Flotation separation of smithsonite from quartz using calcium lignosulphonate as a depressant and sodium oleate as a collector*. Miner. Eng. 131, 385-391.

LIU, W.G., PENG, X.Y., LIU, W.B., ZHANG, N.X., WANG, X.Y., 2022. *A cost-effective approach to recycle serpentine tailings: Destruction of stable layered structure and solvent displacement crystallization*. Int. J. Min, Sci. Techno. 32, 595-603.

LUO, B., NIE, W.L., DONG, J.S., 2022. *Effect of lead ions on the sulfidization flotation of smithsonite using sodium butyl xanthate as a collector*. Miner. Eng. 185, 107710.

LUO, Q. Y., SHI, Q., LIU, D.Z., LI, B.B., JIN, S.Z., 2022. *Effect of deep oxidation of chalcopyrite on surface properties and flotation performance*. Int. J. Min, Sci. Techno. 32, 907-914.

LV, L., WANG, X., REN, H., LIU, J., ZHU, Y. M., 2021. *Depressing behaviors and mechanism of an eco-friendly depressant on flotation separation of cassiterite and fluorite*. J. Mol. Liq. 322, 114898.

MWEENE, L., KHANAL, G.P., NAMBAJE, C., 2021. *Experimental study on the separation of quartz from pyrite using alginate as a selective depressant substantiated by theoretical analysis on intermolecular bonding*. Sep. Purif. Technol. 276, 119251.

NAKLICKI, M.L., RAO, S.R., GOMEZ, M., FINCH, J.A., 2002. *Flotation and surface analysis of the nickel (II) oxide/amyl xanthate system*. Int. J. Miner. Process. 65, 73-82.

NOWOSIELSKA, A.M., NIKOLOSKI, A.N., PARSONS, D.F., 2022. *Interactions between coarse and fine galena and quartz particles and their implications for flotation in NaCl solutions*. Miner. Eng. 183, 107591.

XIE, R.Q., ZHU, Y.M., LIU, J., LI, Y.J., 2021. *The flotation behavior and adsorption mechanism of a new cationic collector on the separation of spodumene from feldspar and quartz*, Sep. Purif. Technol. 264, 118445.

XIE, R.Q., ZHU, Y.M., LIU, J., LI, Y.J., 2021. *Effects of metal ions on the flotation separation of spodumene from feldspar and quartz*. Miner. Eng. 168, 106931.

XIE, R.Q., ZHU, Y.M., LIU, J., LI, Y.J., 2021. *Flotation behavior and mechanism of a-bromododecanoic acid as collector on the flotation separation of spodumene from feldspar and quartz*. J. Mol. Liq. 336, 116303.

WANG, Y.F., KHOSO, S.A., LUO, X.M., TIAN, M.J., 2019. *Understanding the depression mechanism of citric acid in sodium oleate flotation of Ca^{2+}-activated quartz: Experimental and DFT study*, Miner. Eng. 140, 105878.

WANG, X., LIU, J., ZHU, Y.M., HAN, Y.X., 2021. *Adsorption and depression mechanism of an eco-friendly depressant PCA onto chalcopyrite and pyrite for the efficiency flotation separation*, Colloid. Surface. A. 620, 126574.

WANG, L., GAO, H.Y., SONG, S.M., ZHOU, W.G., XUE, N., NIE, Y.M., FENG, B., 2021. *The depressing role of sodium alginate in the flotation of Ca^{2+}-activated quartz using fatty acid collector*. J. Mol. Liq. 343, 117618.

WANG, H., FENG, L.Y., MANICA, R., LIU, Q.X., 2021. *Selective depression of millerite (β-NiS) by polysaccharides in alkaline solutions in Cu-Ni sulphides flotation separation*, Miner. Eng. 172, 107139.

WANG, L., WANG, G.D., GE, P., SUN, W., TANG, H.H., HU, W.J.H., 2022. *Activation mechanisms of quartz flotation with calcium ions and cationic/anionic mixed collectors under alkalescent conditions*. Colloid. Surface. A. 632, 127771.

WANG, H., HAN, J.A., MANICA, R., QI, C., LIU, Q.X., 2022. *Effect of Cu(II) ions on millerite (β-NiS) flotation and surface properties in alkaline solutions*. Miner. Eng. 180, 107443.

WANG, M.T., ZHANG, G.F., ZHAO, L., CHEN, Y.F., LIU, D.Z., LI, C.B., 2022. *Application of eco-friendly tetrasodium iminodisuccinate for separation of smithsonite from zinc ions activated quartz*. Miner. Eng. 181, 107545.

WATLING, H.R., 2008. *The bioleaching of nickel-copper sulfides*. Hydrometallurgy. 91, 70-88.

YANG, S.Y., WANG, L.G., 2019. *Measurement of froth zone and collection zone recoveries with various starch depressants in anionic flotation of hematite and quartz*. Miner. Eng. 138, 31-42.

ZHANG, Q., WEN, S.M., FEN, Q.C., LIU, Y.B., 2021. *Activation mechanism of lead ions in the flotation of sulfidized azurite with xanthate as collector*. Miner. Eng. 163, 106809.

ZHANG, Q., WEN, S.M., NIE, W.L., FENG, Q.C., 2022. *Effect of dissolved species of cerussite on quartz flotation in sulfidization xanthate system*. J. Mol. Liq. 356, 119055.

ZHANG, Q., WEN, S.M., NIE, W.L., FENG, Q.C., 2022. *Effect of dissolved species of cerussite on quartz flotation in sulfidization xanthate system*. J. Mol. Liq. 365, 119055.

ZHANG, Y., ZHANG, X.L., LIU, X.X., CHANG, T.C., NING, S., SHEN, P.L., LIU, R.Z., LAI, H., LIU, D.W., YANG, X.Y, 2022. *Carrageenan xanthate as an environmental-friendly depressant in the flotation of Pb–Zn sulfide and its underlying mechanism*, Colloid. Surface. A. 653, 129926.

ZHAO, K.L., YAN, W., WANG, X.H., WANG, Z., GAO, Z.Y., WANG, C.Q., HE, W., 2020. *Effect of a novel phosphate on the flotation of serpentine-containing copper-nickel sulfide ore*. Miner. Eng. 150, 106276.

ZHAO, L., ZHANG, G.F., WANG, M.T., ZHENG, S.Y., LI, B.B., 2022. *Selective separation of smithsonite from quartz by using sodium polyaspartate as a depressant*. Colloid. Surface. A. 644, 128840.

ZHAO, W.J., WANG, M.L., YANG, B., FENG, Q.C., LIU, D.W., 2022. *Enhanced sulfidization flotation mechanism of smithsonite in the synergistic activation system of copper–ammonium species*. Miner. Eng. 187, 107796.

ZHOU, C.Y., LIU, L.Y., CHEN, J., MIN, F.F., LU, F.Q., 2022. *Study on the influence of particle size on the flotation separation of kaolinite and quartz*. Powder Technol. 408, 117747.